Probabilistic Analysis of Spectral Efficiency for LTE Based on PDCCH Measurement Data

Yoonjoo Lee, Yunbae Kim, Yeongyu Park, and Seungkeun Park

***Abstract*— As the number of mobile subscribers of long-term evolution (LTE) service increases, it becomes important for various parties, such as operators, policymakers, and researchers, to examine how well LTE cells are deployed in terms of actual performance. To this end, we focus on spectral efficiency (SE) with the cell edge user throughput (TP) and average cell SE which can be calculated from the spectrum data of an LTE physical downlink control channel decoding device—Rohde & Schwarz TSME. For these two aspects, crucial probabilities for the performance evaluations are defined using a joint distribution of resource block utilization and cell TP. We derive novel transformation methods that make them approximately follow a joint Gaussian distribution and use it to compute the probabilities. Furthermore, a deep neural network is adopted to analyze not only limited cases but also a wider range.**

***Index Terms*— LTE, resource block, cell edge throughput, cell spectral efficiency, deep neural network.**

I. Introduction

LONG Term Evolution (LTE) has become mature enough to provide connectivity for most terrestrial mobile users. Thus, a careful evaluation of how well the cell deployment is made to provide sufficient services to users is required from various perspectives such as LTE operators, policy makers on spectrum resource, and academic researchers. Spectral Efficiency (SE) is an important indicator of how efficiently the cells are deployed. Although the SE performance can be analyzed accurately by using the up/downlink signal information accumulated on the operators' side, they are reluctant to release the relevant data. Thus it has been preferred to perform the evaluation through in-field measurement without operators' support [1]–[6].

In this work, we focus on the cell edge user ThroughPut (TP) and Cell SE (CSE), which are targeted with higher priority for SE of LTE system [7]. Since the notion of 'efficiency' means how many information bits are delivered in a certain amount of spectrum, TP and Resource Block (RB) utilization should be considered at the same time for SE analysis. Considering a certain level of required TP for cell edge users, we try to derive the probability that at least one user cannot experience the required TP when the number of users and RB utilization in the cell are given. CSE, measured in bps/Hz/cell, is probably the most important parameter that defines the actual capacity of the system. It is defined as the aggregate TP of users normalized by the channel bandwidth and the number of cells. The value of CSE depends on the channel conditions of users, and various techniques exploiting users' channel variations to enhance CSE have been discussed [8]. Thus, the CSE performance can be assessed from a probabilistic point of view such as stochastic ordering, and we try to derive a probability distribution of the CSE for a given number of users.

The information required for the SE analysis mentioned above is how many bits each user receives via how many RBs. In order to obtain such information through measurement, it is common to track the performance of each connected user device. For this purpose, softwares, such as *MobileInsight* [4] and *NETIMIZER* Diagnostic Monitor Logger & Analyzer, that can be run on off-the-shelf smartphones have been utilized [5], [6]. These approaches allow us to collect specific information, such as channel condition, as well as allocated bits and RBs from each user's perspective. However, as the SE analysis requires the information of all users simultaneously, there is a difficulty in tracking all devices at the same time. According to 3GPP releases, Physical Downlink Control CHannel (PDCCH) of LTE downlink signal contains scheduling information on how many bits are transmitted to users through which RB configurations. To exploit this, there have been works on developing platforms, such as *LTEye* [1] and *OWL* [2], that can sniff downlink signal and decode PDCCH to parse such information [3]. These works could be independent of the support from operators by utilizing their own radio devices, chipsets, and processors. In this work, to relieve the burden of developing such a platform directly, we use a well-known off-the-shelf scanner called TSME, which also can decode LTE PDCCHs for verifying network deployment [9]. It comes with ROMES software and we analyze the SE performance using the data obtained from it.

In this Letter, we provide a methodology for analyzing SE using the data acquired through TSME and ROMES. The data used for the analysis were collected for four days (20th April, 4th, 18th, and 25th May, 2018) at a subway station in Seoul, which is the capital of Korea, where the floating population is high. We focus on two bands: 'Band 1' at sub-GHz frequency with 10MHz bandwidth and 'Band 2' at a frequency between 1GHz and 2GHz with 20MHz bandwidth. The data includes the number of Radio Network Temporary Identifiers (RNTIs), RB utilization, and cell TP. As mentioned above, the SE analysis requires all the three features, and we

Manuscript received May 25, 2019; accepted June 19, 2019. Date of publication June 28, 2019; date of current version September 10, 2019. This work was supported by Institute for Information & communications Technology Promotion (IITP) grant funded by the Korea government (MSIT) (No.2017-0-00109, Development of Frequency Analysis Technology for the Virtuous Circulation of Radio Resource). The associate editor coordinating the review of this letter and approving it for publication was O. Popescu. *(Corresponding author: Yunbae Kim.)*

The authors are with the Radio Resource Research Group, Electronics and Telecommunications Research Institute (ETRI), Daejeon 34129, South Korea (e-mail: yjl7436@gmail.com; doko9gum@etri.re.kr; ygp60157@etri.re.kr; seungkp@etri.re.kr).

Digital Object Identifier 10.1109/LCOMM.2019.2925790

express the probabilities associated with the analysis using the conditional joint distribution of RB utilization and cell TP given the number of RNTIs. To take advantages of the property that a joint Gaussian is entirely characterized by the first and second moments, through careful investigation of the empirical distribution of data, we devise widely applicable transformations by which the results are approximately jointly Gaussian. Also, noting that our data does not cover every case of cell configurations, we adopt a Deep Neural Network (DNN) with a standard multilayer structure as a universal function approximator [10].

II. Data Processing

In this section, we explain how the data is processed and transformed for our analysis. Although TSME is capable of decoding PDCCH, it is not performed on every subframe, and the decoded information can only be accessed through ROMES. Thus, it is hard to deal with the raw data itself directly. Instead, ROMES extracts statistical results for raw data obtained over a predefined Observation Interval (OI) of at least five seconds into a Microsoft Excel format. In this work, we use three features as follows. The ‘Number of RNTIs’ denoted as N means the number of different RNTIs found during the OI. The ‘RB usage of Cell’ denoted as R means the ratio of the sum of all scheduled RBs to the sum of total RBs in measured subframes during the OI. The ‘Average Scheduled TP of Cell’ denoted as T means the ratio of the sum of all transmitted bits to the number of measured subframes during the OI. R takes a value between 0 and 1, and T takes a value in kbps unit. From now on, we regard N, R, and T as random variables.

In this work, we aim to compare SE performances according to the number of users served in a cell. Such performances can be described by using a joint probability distribution of (R, T) given N. We first fix a band. TSME can scan multiple cells of the same band if the received signals from the cells are strong enough to be decoded at the location of measurement. Since we focus on the per-cell performance, all the data are aggregated regardless of the cells from which the data is obtained and the days of measurement. Let the set of all the data be $\mathcal{D}$ consisting of (r, t, n) triples of realized values for R, T, and N. For the analysis, we first categorize the extracted data by the number of users, and let $\mathcal{D}_n$ be the set of (r, t) pairs where $N = n$, i.e., $\mathcal{D}_n = \{(r, t) : (r, t, n) \in \mathcal{D}\}$. When the conditional joint distribution follows a joint Gaussian, we can fully describe the probabilistic structure using only the first and second moments. We can expect that R and T follow Gaussian distributions because these are sample means of the decoded values from measured subframes, but the actual data does not show normality as shown in Fig. 1 and Fig. 3 and even shows high time correlations in that the data has multiple runs of the same values. Therefore, in order to utilize the data as a random sample, we randomly choose a set of pairs of certain size K from $\mathcal{D}_n$ to describe the conditional joint distribution $(R, T)|N = n$. For the chosen samples, we try to devise transformations that make the transformed results approximately follow a joint Gaussian to take its advantage mentioned earlier. Also, considering bijective maps for the transformations, we facilitate the calculation of interested probabilities using Gaussian distributions. In the following, we use the notations σ_X^2 and σ_{XY} to indicate the variance of X and the covariance of X and Y, respectively, for generic random variables X and Y.

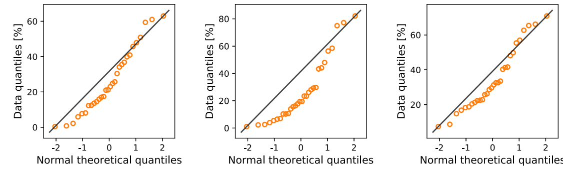

(a) $N = 4$ (b) $N = 6$ (c) $N = 8$

Fig. 1. Q-Q plots of R given $N = 4$, 6, and 8 in Band 1 against the theoretical quantiles of $\mathcal{N}(0, 1)$. Samples of size $K = 30$ are chosen.

A. Transformation of RB Utilization

Here, we provide a way to transform R so that the transformed result can be approximated to follow a standard Gaussian $\mathcal{N}(0, 1)$. As can be seen in the Q-Q (quantile-quantile) plots given in Fig. 1, $R|N = n$ shows ‘S’-shaped quantiles against normal theoretical quantiles in general. For $1 \leq k \leq K$, we take $\Phi^{-1}\left((k - 0.375)/(k + 0.25)\right)$, denoted by q_k, for normal theoretical quantiles as highly recommended in [11]. The function $\Phi(\cdot)$ indicates the cumulative distribution function (cdf) of $\mathcal{N}(0, 1)$. Typically ‘S’-shaped Q-Q plot implies that the data have thicker tails or flatter distribution than $\mathcal{N}(0, 1)$. Thus, it is reasonable to transform R in the way of compressing the middle and expanding both tails. In this regard, our proposed family of functions $G(r; a, b, c)$ for the transformation is given as $G(r; a, b, c) = a \log(r) - b \log(1 - r) + c$, where $a \geq 0$, $b \geq 0$, and $c \in \mathbb{R}$ for the monotonicity of transformation. These functions can control where to compress and expand by tuning the parameters (a, b, c). Let $\{r_k\}_{1 \leq k \leq K}$ be the chosen samples for R sorted in ascending order. We find the parameters (a, b, c) that minimizes the following:

$$J_R(a, b, c) = \sum_{k=1}^{K} \left\{ q_k - G\left(r_k; a, b, c\right) \right\}^2 . \tag{1}$$

Note that, since the functions that are squared and summed in (1) are affine transformations of (a, b, c) and the square operation is convex, $J_R(a, b, c)$ is convex. Optimal values for (a, b, c) can be easily obtained by equating the gradient of $J_R(a, b, c)$ to zero with some manipulations for meeting the parameter conditions $a \geq 0$ and $b \geq 0$. For convenience, we define three random variables Q, L, and M taking values on $\{q_k\}$, $\{\log(r_k)\}$, and $\{\log(1 - r_k)\}$, respectively, with uniform probabilities $P(Q = q_k) = P(L = \log(r_k)) = P(M = \log(1 - r_k)) = 1/K$ for $1 \leq k \leq K$. The values $D_R = \sigma_M^2 \sigma_{LQ} - \sigma_{LM} \sigma_{MQ}$ and $\hat{D}_R = \sigma_{LM} \sigma_{LQ} - \sigma_L^2 \sigma_{MQ}$ serve as kinds of discriminant on parameter conditions. Then we have the optimal values for (a, b, c) as given in the upper part of Table. I. Fig. 2 illustrates the Q-Q plots of transformed results for the data shown in Fig. 1. We can check from the figure that the transformed quantiles are aligned with theoretical ones.

TABLE I
OPTIMAL PARAMETERS FOR TRANSFORMATIONS

R	$D_R < 0$	$\hat{D}_R < 0$	otherwise
a	0	σ_{LQ}/σ_L^2	$D_R/\left\{\sigma_L^2\sigma_M^2 - (\sigma_{LM})^2\right\}$
b	$-\sigma_{MQ}/\sigma_M^2$	0	$\hat{D}_R/\left\{\sigma_L^2\sigma_M^2 - (\sigma_{LM})^2\right\}$
c	$E[Q] - aE[L] + bE[M]$		
T	$D_T < 0$	$\hat{D}_T < 0$	otherwise
d	0	σ_{OQ}/σ_O^2	$D_T/\left\{\sigma_O^2\sigma_{T'}^2 - (\sigma_{OT'})^2\right\}$
e	$\sigma_{T'Q}/\sigma_{T'}^2$	0	$\hat{D}_T/\left\{\sigma_O^2\sigma_{T'}^2 - (\sigma_{OT'})^2\right\}$
f	$E[Q] - dE[O] - eE[T']$		

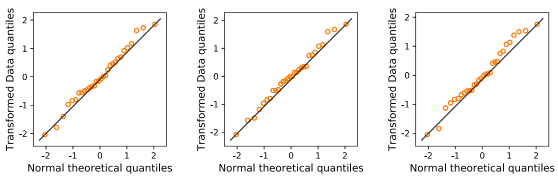

(a) $N = 4$ (b) $N = 6$ (c) $N = 8$

Fig. 2. Q-Q plots of the values transformed from the data shown in Fig. 1.

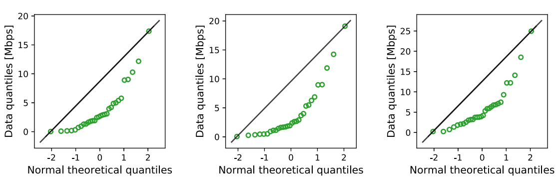

(a) $N = 4$ (b) $N = 6$ (c) $N = 8$

Fig. 3. Q-Q plots of T given $N = 4$, 6, and 8 in Band 1 against the theoretical quantiles of $\mathcal{N}(0, 1)$. Samples of size $K = 30$ are chosen.

B. Transformation of Cell TP

Here, we provide a transformation method that makes the transformed T approximately follow $\mathcal{N}(0, 1)$. Fig. 3 shows that $T|N = n$ has quantiles arced below theoretical quantiles in general. Since such types of quantiles imply right-skewed distributions of data, it is reasonable to expect that transformations expanding the left tail and compressing the right tail work well. Our proposed family of functions $H(t; d, e, f)$ for the transformation is given by $H(t; d, e, f) = d\log(t) + et + f$, where $d \geq 0$, $e \geq 0$, and $f \in \mathbb{R}$ for the monotonicity of transformation. The linear term is added to regularize compressing the right tail. Deriving optimal parameters (d, e, f) for the transformation is similar to the processes given in the previous section. With the chosen samples $\{t_k\}_{1 \leq k \leq K}$ for T sorted in ascending order, the cost function $J_T(d, e, f)$ we want to minimize is defined as follows:

$$J_T(d, e, f) = \sum_{k=1}^{K} \left\{q_k - H\left(t_k; d, e, f\right)\right\}^2.$$

Optimal values for (d, e, f) also can be easily obtained in a similar way to the case of deriving (a, b, c) for R. For convenience, we define two random variables O and T' taking values on $\{\log(t_k)\}$ and $\{t_k\}$, respectively, with uniform probabilities. The values $D_T = \sigma_{T'}^2\sigma_{OQ} - \sigma_{OT'}\sigma_{T'Q}$ and $\hat{D}_T = \sigma_O^2\sigma_{T'Q} - \sigma_{T'O}\sigma_{OQ}$ serve as kinds of discriminant on parameter conditions. Then we have the optimal values for (d, e, f) as given in the lower part of Table. I. The validity of our transformation can be checked from Fig. 4.

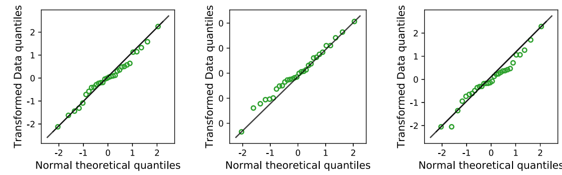

(a) $N = 4$ (b) $N = 6$ (c) $N = 8$

Fig. 4. Q-Q plots of the values transformed from the data shown in Fig. 3.

C. Processing Data for SE Analysis

So far, we have discussed how to transform (R, T) so that the marginals are approximately Gaussian. The validity of the transformations can be verified statistically by performing a normality test. However, since marginal normalities do not imply the joint normality, a test for joint normality should also be applied. Due to the high time correlations of the data mentioned above, a small value of K is favorable in that the chosen data can be regarded as a random sample. Hence, we use Shapiro-Wilk and Royston tests for marginal and joint normalities, respectively, which are recommended in terms of power, the probability of correct rejection, for a small number of sample sizes [12], [13]. A significance level of 0.05 is used for the tests.

Now we describe the details of processing data for analysis. We use the notation $|\mathcal{A}|$ for a set $\mathcal{A}$ to indicate its cardinality. First, we choose a sample for N with probabilities $P(N = n) = |\mathcal{D}_n|/|\mathcal{D}|$. If n is chosen for N, we randomly choose a sample $\{(r_k, t_k)\}_{1 \leq k \leq K}$ of size K for $(R, T)|N = n$ from $\mathcal{D}_n$. And, we derive optimal transformation parameters (a, b, c, d, e, f) as described in Section II-A and II-B. For the transformed data $\{G(r_k;\ a,\ b,\ c)\}$ and $\{H(t_k;\ d,\ e,\ f)\}$, we perform Shapiro-Wilk test separately. If the null hypothesis of normality is accepted, we assume that these are random samples from $\mathcal{N}(0, 1)$. Also, for testing joint normality, Royston test is performed on the set of pairs $\{(G(r_k; a, b, c), H(t_k; d, e, f))\}$. If the null hypothesis is also accepted, we assume that the set of pairs is a random sample from a joint Gaussian $\mathcal{N}\left(\left[\begin{smallmatrix}0\\0\end{smallmatrix}\right], \left[\begin{smallmatrix}1 & \rho\\ \rho & 1\end{smallmatrix}\right]\right)$ where ρ is the sample covariance. Fig. 5 illustrates the histograms of marginals and the scatter plots of joints for transformed results from the data shown in Fig. 1 and Fig. 3 for which the null hypotheses are all accepted. Observing the plots and p-values given in Fig. 5, we can check that the data obtained from the process approximately follow a joint Gaussian. Then, we set $(n, \boldsymbol{\theta})$ be a data point where $\boldsymbol{\theta} = (a, b, c, d, e, f, \rho)$. If the null hypothesis is rejected in one of the tests above, we start by choosing another sample from N again. The procedure described here is summarized in the flowchart given in Fig. 6. From now on, we use $G(R; \boldsymbol{\theta})$ and $H(T; \boldsymbol{\theta})$ to indicate $G(R; a, b, c)$ and $H(T; d, e, f)$, respectively.

III. CELL EDGE PERFORMANCE ANALYSIS

Let the required TP for cell edge users be given as α in kbps unit. Then, for given $N = n$ and $R = r$, the probability

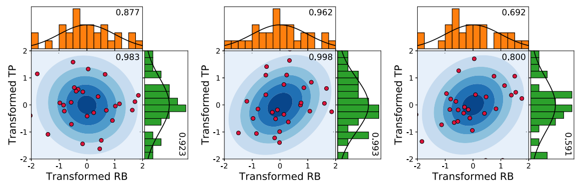

(a) $N = 4$ (b) $N = 6$ (c) $N = 8$

Fig. 5. The histograms of marginals and the scatter plots of joints for transformed R and T given $N = 4$, 6, and 8 shown in Fig. 2 and Fig. 4. The upper left panel shows the histogram of R with the pdf $\mathcal{N}(0,1)$ indicated by the curve. The lower right panel is for T. The lower left panel shows the scatter plot for transformed pairs with the level curves of the joint Gaussian. The values on the upper right side of the panels are the p-values of respective normality tests.

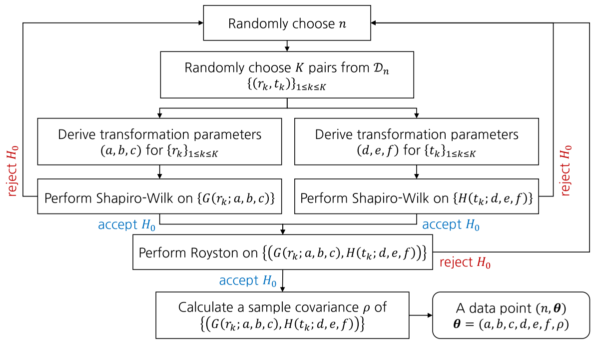

Fig. 6. A flowchart for data processing.

of interest can be described as follows:

$$P_m(\alpha,n,r) = P\left(T < \alpha n | N = n, R = r\right). \tag{2}$$

This is because $P_m(\alpha,n,r)$ is the probability that at least one user cannot experience αkbps when the cell is serving n users utilizing $(100r)\%$ of total RBs. If transformations $G(R)$ and $H(T)$ so that $(G(R), H(T))|N = n$ approximately follows a joint Gaussian $\mathcal{N}\left(\left[\begin{smallmatrix}0\\0\end{smallmatrix}\right], \left[\begin{smallmatrix}1 & \rho\\ \rho & 1\end{smallmatrix}\right]\right)$ are given, the conditional distribution for $H(T)|N = n, R = r$, equivalently $H(T)|N = n, G(R) = G(r)$, can be approximated to follow a Gaussian $\mathcal{N}\left(\rho G(r), 1-\rho^2\right)$. Then, $P_m(\alpha,n,r)$ in (2) can be computed as follows.

$$\begin{aligned} P_m(\alpha,n,r) &= P\left(H(T) < H\left(\alpha n\right) | N = n, G(R) = G(r)\right) \\ &\quad (\because\ H(\cdot) \text{ and } G(\cdot) \text{ are strictly increasing}) \\ &= P\Big(\frac{H(T) - \rho G(r)}{\sqrt{1-\rho^2}} \\ &\quad < \frac{H\left(\alpha n\right) - \rho G(r)}{\sqrt{1-\rho^2}} \Big| N = n, G(R) = G(r)\Big) \\ &= \Phi\left(\frac{H\left(\alpha n\right) - \rho G(r)}{\sqrt{1-\rho^2}}\right). \end{aligned} \tag{3}$$

Here, we calculate the probability using our data. We exploit DNNs to predict the probability for any case, whether it is measured or not. We first describe how to construct input-output pairs for DNN learning. Assume that we are equipped with data points of size Λ, which are generated via the method given in Section II-C. For a data point $(n, \boldsymbol{\theta})$, to make an input for calculating the probability of interest, we randomly generate values for α and r. Considering typical data rates for streaming video of 720p or less quality [14], α is chosen from $\mathcal{U}(500, 4000)$, where $\mathcal{U}$ indicates a uniform distribution. Also, considering the cells where more than 40% of RBs are utilized, r is chosen from $\mathcal{U}(0.4, 1)$. Then, we have an input as (α, n, r). For the output, we calculate the argument in (3) with $\boldsymbol{\theta}$ as $y_m(\alpha,n,r;\boldsymbol{\theta}) = \{H\left(\alpha n;\boldsymbol{\theta}\right) - \rho G(r;\boldsymbol{\theta})\}/\sqrt{1-\rho^2}$. In this way, an input-output pair can be made for each of the Λ data points.

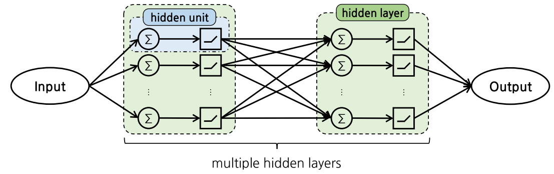

Fig. 7. Structure of a standard multilayer feedforward network.

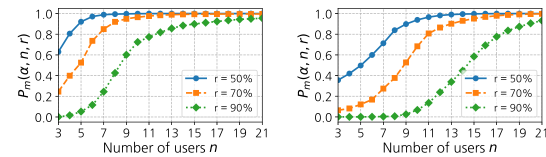

(a) Band 1 (b) Band 2

Fig. 8. Predicted probabilities of interest for various cases with $\alpha = 2$Mbps.

For DNN learning, we adopt the standard multilayer feedforward structure given in Fig. 7. For simplicity, we have omitted bias terms in the figure. Rectified Linear Unit, which is the most popular in modern NNs [15], is used as the activation function of hidden units. Among the Λ input-output pairs, 60% of them are utilized as a train data set and the rest are used as a validation data set for applying the 'Early Stopping' technique. Once a model is established after the learning, the probability for any input (α, n, r) can be calculated simply by putting the corresponding output of the model into $\Phi(\cdot)$.

Fig. 8 shows the prediction results for various cases. For the results, $K = \min\{30, |\mathcal{D}_n|/2\}$ is used when $N = n$. We generated $\Lambda = 10000$ data points. The numbers of hidden layers and hidden units for each layer are set to 45 and 64, respectively. The figure shows the overall tendency of increasing probability as the number of users increases and the RB utilization decreases as expected. In other words, if a large number of users are served through insufficient RBs, it is likely that there are users who do not achieve the required TP. Also the overall lower probabilities in Fig. 8-(b) than in Fig. 8-(a) show that our approach naturally reflects that the operating bandwidth of Band 2 is wider than that of Band 1. Furthermore, we can check that the prediction by the DNN model shows consistent results for all cases whether they are in the data (e.g., $n \le 11$ and ≤ 18 for Band 1 and 2, respectively) or not.

IV. Cell Spectral Efficiency Analysis

In this section, we provide a way to derive and calculate a complementary cdf (ccdf) of CSE using the random variables defined in Section II. Letting w be the bandwidth in kHz unit, CSE S can be defined as $T/(wR)$. If the transformations $G(\cdot)$

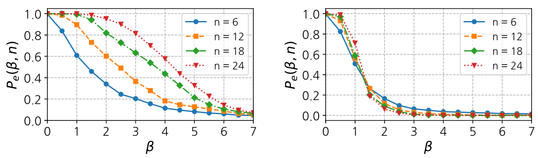

(a) Band 1 (b) Band 2

Fig. 9. Predicted ccdf of CSE for various cases.

and $H(\cdot)$ are given as in Section III, the ccdf $P_e(\beta, n)$ for $S|N = n$ can be computed as follows.

$$\begin{aligned}
P_e(\beta, n) &= P(S > \beta | N = n) = P\left(\frac{T}{wR} > \beta \middle| N = n\right) \\
&= P\left(\frac{T}{G^{-1}(G(R))} > w\beta \middle| N = n\right) \\
&\quad (\because\ G \text{ is strictly increaing}) \\
&= P\left(H(T) > H\left(G^{-1}(G(R))w\beta\right) | N = n\right) \\
&\quad (\because\ H \text{ is strictly increaing}) \\
&= \int_{-\infty}^{\infty} \int_{H(G^{-1}(u)w\beta)}^{\infty} f_{G(R),H(T)|N=n}(u, v)\,dv\,du \\
&= \int_{-\infty}^{\infty} \left(\int_{H(G^{-1}(u)w\beta)}^{\infty} f_{H(T)|G(R),N=n}(v|u)\,dv \right) \\
&\quad f_{G(R)|N=n}(u)\,du \\
&= \int_{-\infty}^{\infty} \left\{ 1 - \Phi\left(\frac{H\left(G^{-1}(u)w\beta\right) - \rho u}{\sqrt{1-\rho^2}} \right) \right\} \\
&\quad f_{G(R)|N=n}(u)\,du. \\
&\quad (\because\ H(T)|G(R) = u, N = n \sim \mathcal{N}\left(\rho u, 1-\rho^2\right))
\end{aligned} \tag{4}$$

Since it is hard to compute the integral (4) in a closed form, we exploit Monte Carlo integration technique. Noting that $G(R)|N = n$ approximately follows $\mathcal{N}(0, 1)$, the integral (4) can be computed as

$$\frac{1}{\Gamma} \sum_{i=1}^{\Gamma} \left\{ 1 - \Phi\left(\frac{H\left(G^{-1}(u_i)w\beta\right) - \rho u_i}{\sqrt{1-\rho^2}} \right) \right\}, \tag{5}$$

where $\{u_i\}_{1 \le i \le \Gamma}$ is a random sample of size Γ from $\mathcal{N}(0, 1)$.

For the calculation of ccdf for any cell configurations, we also utilize a DNN as in Section III. We begin with the same set of data points of size Λ as above. For a data point $(n, \boldsymbol{\theta})$, an input is configured by associating n with β and u, which are random samples from $\mathcal{U}(0, 10)$ and $\mathcal{N}(0, 1)$, respectively. For this input (β, n, u), an output is set to the argument of $\Phi(\cdot)$ in (4) with $\boldsymbol{\theta}$ as $y_e(\beta, n, u; \boldsymbol{\theta}) = \left\{H\left(G^{-1}(u; \boldsymbol{\theta})w\beta; \boldsymbol{\theta}\right) - \rho u\right\} / \sqrt{1-\rho^2}$. Here, we also use the same DNN structure given in Fig. 7. After the DNN learning, we can compute each summand in (5) for any input (β, n, u) by putting the corresponding output of the learned model into $1 - \Phi(\cdot)$.

Fig. 9 shows the results of CSE for various cases. Here we use the same K and Λ as in Section III. To train a DNN model, we use 5 layers and 20 units for Band 1, and 15 layers and 32 units for Band 2. For the calculation of (5), we set $\Gamma = 500$. As can be seen in the figure, the effect of multiuser diversity in Band 1 is more conspicuous than in Band 2. Also, an overall tendency that the CSE of Band 1 is higher than that of Band 2 is observed. So it can be checked that our approach accurately catches the fact that Band 1 has more favorable channel conditions than Band 2, which is consistent with the measurement results given in [6]. Furthermore, as in the previous section, the prediction results by DNN for the cases not measured keep the tendency appeared in the results for measured cases.

V. Conclusion

In this Letter, we provided a method to analyze SE for deployed LTE cells. The analysis was based on in-field measurement data with a well-known LTE scanner. We devised novel transformations for RB utilization and cell TP which make the results approximately follow Gaussian distributions. The transformations enabled us to describe the key probabilities for SE analysis through a joint Gaussian. Also, DNNs were adopted to extend the analysis from the measured cases to general cases. The presented approach is generally applicable because it reflects the stochastic characteristics of RB utilization and downlink TP from the measurement data. Thus, we expect the proposed method to be used in examining the appropriateness of LTE cell deployments.

References

[1] S. Kumar, E. Hamed, D. Katabi, and L. E. Li, "LTE radio analytics made easy and accessible," in *Proc. ACM Conf. SIGCOMM*, Aug. 2014, pp. 211–222.

[2] N. Bui and J. Widmer, "OWL: A reliable online watcher for LTE control channel measurements," in *Proc. 5th Workshop All Things Cellular, Oper., Appl. Challenges*, Oct. 2016, pp. 25–30.

[3] R. Falkenberg, K. Heimann, and C. Wietfeld, "Discover your competition in LTE: Client-based passive data rate prediction by machine learning," in *Proc. IEEE GLOBECOM*, Dec. 2017, pp. 1–7.

[4] Y. Li, C. Peng, Z. Yuan, J. Li, H. Deng, and T. Wang, "MobileInsight: Extracting and analyzing cellular network information on smartphones," in *Proc. 22nd Annu. Int. Conf. Mobile Comput. Netw.*, Oct. 2016, pp. 202–215.

[5] S. Park, M. Agiwal, H. Kwon, and H. Jin, "An evaluation methodology for spectrum usage in LTE-A networks: Traffic volume and resource utilization perspective," *IEEE Access*, vol. 7, pp. 67863–67873, 2019.

[6] P. M. Sainju, "LTE performance analysis on 800 and 1800 MHz bands," M.S. thesis, Dept. Commun. Eng., Tampere Univ. Technol., Tampere, Finland, 2012.

[7] *LTE; Requirements for Further Advancements for Evolved Universal Terrestrial Radio Access (E-UTRA) (LTE-Advanced) (Release 15)*, document TR 36.913, 3GPP, 2010.

[8] F. Boccardi, B. Clerckx, A. Ghosh, E. Hardouin, G. Jöngren, K. Kusume, E. Onggosanusi, and Y. Tang, "Multiple-antenna techniques in LTE-advanced," *IEEE Commun. Mag.*, vol. 50, no. 3, pp. 114–121, Mar. 2012.

[9] J. Schilbach, "R&STSMW, TSME, TSMA LTE downlink allocation analysis," Appl. Note Rohde & Schwarz, Munich, Germany, 2016.

[10] M. Leshno, V. Y. Lin, A. Pinkus, and S. Schocken, "Multilayer feedforward networks with a nonpolynomial activation function can approximate any function," *Neural Netw.*, vol. 6, no. 6, pp. 861–867, 1993.

[11] G. Blom, *Statistical Estimates and Transformed Beta-Variables*. New York, NY, USA: Wiley, 1958.

[12] N. M. Razali and Y. B. Wah, "Power comparisons of Shapiro-Wilk, Kolmogorov-Smirnov, Lilliefors and Anderson-Darling tests," *J. Stat. Model. Anal.*, vol. 2, no. 1, pp. 21–33, Jan. 2011.

[13] P. J. Farrell, M. Salibian-Barrera, and K. Naczk, "On tests for multivariate normality and associated simulation studies," *J. Stat. Comput. Simul.*, vol. 77, no. 12, pp. 1065–1080, Nov. 2005.

[14] F. Wamser, M. Seufert, P. Casas, R. Irmer, P. Tran-Gia, and R. Schatz, "YoMoApp: A tool for analyzing QoE of YouTube HTTP adaptive streaming in mobile networks," in *Proc. Eur. Conf. Netw. Commun. (EuCNC)*, Paris, France, Jun./Jul. 2015, pp. 239–243.

[15] I. Goodfellow, Y. Bengio, and A. Courville, *Deep Learning*. Cambridge, MA, USA: MIT Press, 2016.